Multi-pulse corona discharges in thunderclouds observed in optical and radio bands

Dongshuai Li[1], Alejandro Luque[2], Nikolai Lehtinen[3], F. J Gordillo-Vazquez[4], Torsten Neubert[5], Gaopeng Lu[6], Olivier Chanrion[7], Hongbo Zhang[8], Nikolai Østgaard[3], and Víctor Reglero[9]

[1]Instituto de Astrofísica de Andalucía (IAA)
[2]Instituto de Astrofísica de Andalucía (IAA)-CSIC
[3]University of Bergen
[4]Instituto de Astrofísica de Andalucía, IAA-CSIC
[5]Department of Solar System Physics, Denmark
[6]School of Earth and Space Sciences, University of Science and Technology of China
[7]National Space Institute (DTU Space)
[8]Institute of Atmospheric Physics, Chinese Academy of Sciences
[9]University of Valencia

November 22, 2022

Abstract

How lightning initiates inside thunderclouds remains a major puzzle of atmospheric electricity. By monitoring optical emissions from thunderstorms, the Atmosphere-Space Interactions Monitor (ASIM) onboard the International Space Station is providing new clues about lightning initiation by detecting Blue LUminous Events (BLUEs), which are manifestations of an enigmatic type of electrical discharge that sometimes precedes lightning and is named "fast breakdown". Here we combine optical and radio observations from a thunderstorm near Malaysia to uncover a new type of event containing multiple optical and radio pulses. We find that the first optical pulse coincides with a strong radio signal in the form of a Narrow Bipolar Event (NBE) but subsequent optical pulses, delayed some milliseconds, have weaker radio signals, possibly because they emanate from a horizontally oriented fast breakdown which does not trigger full-fledged lightning. Our results cast light on the differences between isolated and lightning-initiating fast breakdown.

Multi-pulse corona discharges in thunderclouds observed in optical and radio bands

Dongshuai Li[1†], Alejandro Luque[1], Nikolai G. Lehtinen[2], F. J. Gordillo-Vázquez[1], Torsten Neubert[3], Gaopeng Lu[4], Olivier Chanrion[3], Hongbo Zhang[5], Nikolai Østgaard[2], Víctor Reglero[6]

[1]Instituto de Astrofísica de Andalucía (IAA), CSIC, Granada, Spain.
[2]Birkeland Centre for Space Science, Department of Physics and Technology, University of Bergen, Bergen, Norway.
[3]National Space Institute, Technical University of Denmark (DTU Space), Kongens Lyngby, Denmark.
[4]CAS Key Laboratory of Geospace Environment, University of Science and Technology of China, Hefei, China.
[5]Key Laboratory of Middle Atmosphere and Global Environment Observation (LAGEO), Institute of Atmospheric Science, Chinese Academy of Sciences, Beijing, China.
[6]Image Processing Laboratory, University of Valencia, Valencia, Spain.

Key Points:

- Optical multi-pulse corona discharges coincide with Narrow Bipolar Events and their subsequent pulses.
- Subsequent optical pulses are related to horizontally oriented fast breakdowns which emitted faint radio signals.
- The class of horizontally oriented fast breakdowns might play a significant role in the initiation of the lightning leaders.

Corresponding author: Dongshuai Li† and Alejandro Luque,
Instituto de Astrofísica de Andalucía (IAA), CSIC, Granada, Spain.
†Present address: National Space Institute, Technical University of Denmark (DTU Space), Kongens Lyngby, Denmark., (dongshuai@space.dtu.dk, aluque@iaa.es)

Abstract

How lightning initiates inside thunderclouds remains a major puzzle of atmospheric electricity. By monitoring optical emissions from thunderstorms, the Atmosphere-Space Interactions Monitor (ASIM) onboard the International Space Station is providing new clues about lightning initiation by detecting Blue LUminous Events (BLUEs), which are manifestations of an enigmatic type of electrical discharge that sometimes precedes lightning and is named “fast breakdown”. Here we combine optical and radio observations from a thunderstorm near Malaysia to uncover a new type of event containing multiple optical and radio pulses. We find that the first optical pulse coincides with a strong radio signal in the form of a Narrow Bipolar Event (NBE) but subsequent optical pulses, delayed some milliseconds, have weaker radio signals, possibly because they emanate from a horizontally oriented fast breakdown which does not trigger full-fledged lightning. Our results cast light on the differences between isolated and lightning-initiating fast breakdown.

Plain Language Summary

One of the biggest mysteries in the atmospheric sciences is to understand how lightning is initiated inside thunderclouds. By combining observations in optical and radio bands, our work uncovers a yet-unreported type of lightning process: multi-pulse corona discharges. For the first time, we cast light on the differences between the isolated and lightning-initiating fast breakdown (an enigmatic type of electrical discharge that is likely present in all lightning initiation events). Our results indicate that there is an unexpected class of horizontally oriented fast breakdown discharges between those that are fully isolated and those that initiate a leader. They have been ignored by all the radio observations so far due to their faint radio signals. However, this would be the class of breakdowns that play a significant role in the initiation of the lightning leaders.

1 Introduction

Narrow bipolar events (NBEs) are short, strong radio pulses emitted by thunderclouds (Smith et al., 1999, 2004). Interferometric (Rison et al., 2016) as well as optical, space-based observations (Soler et al., 2020; Li et al., 2021) indicate that their source, with an spatial extent of hundreds of meters to a few kilometers and a duration of some tens of microseconds, is a poorly understood type of electrical breakdown produced by the simultaneous propagation of 10^8 to 10^9 cold filamentary discharges called streamers (Li et al., 2021; N. Liu et al., 2019; Nijdam et al., 2020). This type of electrical discharge, called fast breakdown, is likely present in all lightning initiation events (Attanasio et al., 2021; Sterpka et al., 2021) and even during flash development, although only under a still undefined set of conditions it is sufficiently strong to manifest itself as an NBE.

NBEs normally occur in isolation (Rison et al., 2016; Kostinskiy et al., 2020) but a small fraction of them, named Initiation-type NBEs (INBEs) (Wu et al., 2014) are the initial event of a lightning flash. Sometimes NBEs are followed by subsequent radio pulses associated with leaders (hot lightning channels); these pulses, sometimes called Initial Breakdown Pulses (IBPs) (e.g., Kostinskiy et al., 2020; Lyu et al., 2019) or Preliminary Breakdown pulses (PBs) (e.g., Kolmašová et al., 2018; Wu et al., 2015), precede by a few milliseconds an intracloud (IC) or cloud-to-ground (CG) lightning discharge. Whereas isolated NBEs are strong emitters of Very High Frequency (VHF) radiation ($3000 - 300\,000$ W) (Rison et al., 2016; Kostinskiy et al., 2020), initiation-type NBEs, even with pulse widths similar to isolated NBEs, present smaller amplitudes and weaker VHF signals ($3 - 300$ W) (Rison et al., 2016; Kostinskiy et al., 2020; Wu et al., 2014; Bandara et al., 2019).

Most of this knowledge about NBEs and fast breakdown derives from radio observations but these have been recently complemented by optical detections from space. The Modular Multispectral Imaging Array (MMIA) instrument of the Atmosphere-Space Interactions Monitor (ASIM), operating since 2018 from the International Space Station (ISS), has detected a large number of Blue LUminous Events (BLUEs) globally (Soler et al., 2021), which are optical pulses with a strong 337 nm signal, associated with streamer discharges, but lacking the 777 nm emissions that would indicate the presence of a hot leader (Soler et al., 2020; Li et al., 2021; F. Liu, Lu, et al., 2021).

Combined radio and optical studies provide strong evidence that every NBE has a BLUE counterpart (Soler et al., 2020; Li et al., 2021; F. Liu, Lu, et al., 2021). Hence BLUEs are another manifestation of fast breakdown.

Novel optical observations help to elucidate the context in which fast breakdown occurs. Soler et al. (2020) found that a significative fraction of BLUEs contained more than one optical pulse with a delay between pulses of a few milliseconds. Here we combine observations from MMIA and from ground-based Very Low Frequency/Low Frequency (VLF/LF) radio sensors to investigate a number of multi-pulse BLUEs from a thunderstorm near Malaysia. We find that in all these events the first optical pulse has an unambiguous NBE counterpart. Remarkably, we also find that the subsequent optical pulses, even though they have optical amplitudes comparable to the leading pulse, are accompanied by faint, sometimes undetectable, radio emissions. The implication is that NBEs are frequently followed by a new type of event that has escaped detection until now. Our observations are compatible with these events being horizontally directed fast breakdown which does not initiate a leader.

2 Instruments and Observations

Since its commissioning in 2018, the Modular Multispectral Imaging Array (MMIA) of the Atmosphere-Space Interactions Monitor (ASIM) has been observing Earth thunderstorms from space in a nadir-viewing geometry from the International Space Station (ISS) (Chanrion et al., 2019; Neubert et al., 2019). MMIA contains three photometers with a sampling rate of 100 ksamples/s: one photometer in the ultraviolet (UV) band at 180-230 nm, one in the near-UV at the strongest spectral line of the nitrogen second positive system (337 nm) and one at the strongest lightning emission band (777.4 nm). The last two photometers are complemented with cameras sensitive to the same wavelengths. The spatial resolution of the cameras on the ground is around 400 m $\times$ 400 m and they have an integration time of 83.3 ms.

Our radio-frequency data comes from a broadband Very Low Frequency/Low Frequency (VLF/LF) magnetic sensor that operates at 400 Hz to 400 kHz and is located at Universiti Teknikal Malaysia Melaka (UTeM), Malacca, Malaysia (Zhang et al., 2016; Ahmad et al., 2017). To compare MMIA and VLF/LF data correcting for MMIA's time uncertainty we matched MMIA pulses with data from the GLD360 lightning detection network (Said & Murphy, 2016), obtaining a time shift for MMIA with respect to the ground-based VLF/LF measurements of (-15.00 ± 0.65) ms (see Figure S1 in Supplemental Material).

On the evening of April 30, 2020, there were 16 Blue LUminous Events (BLUEs) simultaneously observed by the 337 nm photometer and its filtered camera of MMIA, as well as the ground-based VLF/LF sensor near Malaysia (Ahmad et al., 2017), with absent or negligible signals in both the 180 - 230 nm photometer and in the 777.4 nm photometer and filtered camera. Among the events, there are 8 single-pulse BLUEs (Soler et al., 2020; Li et al., 2021) and 8 multiple-pulse BLUEs. We focus mainly on the multiple-pulse BLUEs.

To illustrate the thunderstorm context of the BLUEs, figure 1 shows the distribution of intracloud (IC)/cloud-to-ground (CG) lightning with the 8 multi-pulsed BLUEs superimposed on the cloud Top Blackbody Brightness Temperature (TBB, given in Kelvin) provided by the Himawari-8 satellite (Bessho et al., 2016) in ten-minute intervals starting at 17:40:00 UTC, 17:50:00 UTC and 18:00:00 UTC. Because GLD360 only captured 3 events, we determine the locations of multiple-pulse BLUEs by projecting the brightest pixel of the of 337-nm camera images into geo-coordinates (latitude and longitude). We also show the GLD360-detected lightning flashes surrounding our events, including their classification as positive or negative, CG or IC. The BLUEs, which occurred in the time period from 17:50:00 to 17:51:00 UTC, are accompanied by the highest concentration of IC and CG lightning with an apparent decrease of the negative CG flash rate.

The detailed features of all multiple-pulse BLUEs are listed in Table 1. As an example, the multiple-pulse BLUE with ID 1 is presented in Figure 2, with other cases given in Figure S2-S9 in the Supplemental Material. The multiple-pulse BLUEs include one primary BLUE pulse and one or several subsequent BLUE pulses within 1 ms to 9 ms. In most cases, both rise time and time duration of the subsequent BLUE pulses are found to be similar or somewhat shorter than those corresponding to the primary BLUEs; the irradiances of the primary BLUEs are higher than those of the subsequent BLUEs pulses by about a factor of two. All the BLUEs are isolated from other IC or CG lightning discharges detected by either GLD360 or the 777.4 nm photometer and filtered camera of MMIA within at least 100 ms. That means that they do not initiate any leader activity and therefore would be classified as isolated NBEs.

3 Results

As shown in Figure 2 and Figures S2-S9 in the Supplemental Material, all the multiple-pulse BLUEs are associated with an isolated positive NBE sometimes accompanied by faint subsequent radio pulse trains. Figure 3 demonstrate the correlation of the horizontal B fields ($B_{\mathbf{EW}}$ and $B_{\mathbf{NS}}$) for both the positive NBE and its subsequent pulses for event 1 (See Figures S11-S19 in Supplemental Materials for other cases).

As shown in figure 3(d), the NBE pulses exhibit a tight linear relationship of the horizontal B fields, something that is expected for the horizontally propagating ground wave of a vertical discharge. However, in the subsequent pulses the horizontal components of the field trace elliptical curves (see Figure 3(h)). As this is a projection into the horizontal plane of the trajectory of the magnetic field in the plane perpendicular to the wave propagation, the implication is that the wave is elliptically polarized. One explanation for this behaviour is that the electric current responsible for the subsequent pulses is oriented horizontally: in that case the ground wave is absent and the first signal to reach the detector is the wave reflected in the ionosphere. Due to the anisotropy introduced by the geomagnetic field, different components of the wave electromagnetic fields propagate differently in the magnetized plasma of the lower ionosphere, introducing a phase shift between different components. This would explain both the weak amplitude and the elliptical polarization of the observed signal.

We tested this hypothesis by means of a Full Wave Method (FWM) electromagnetic model (Lehtinen & Inan, 2008, 2009) (see Methodology in Supplemental Material for further details). We simulated the signals produced by both vertical and horizontal dipole current sources imitating the event-detector geometry of our observations. The results, shown in figure 3, reproduce the qualitative features of the waveform measured by the ground-based VLF/LF. For the case of NBE, both ground wave and its first and second reflected sky waves can be clearly seen in figure 3(a, c) with a linear relationship between the magnetic field components B_x and B_y (see figure 3(b, d)) . For the subsequent pulse trains, the ground wave is absent and the magnetic field components B_x and B_y of the first and second sky waves trace elliptical curves (see figure 3(e,f,g,h)). These simulations support our hypothesis of a horizontal discharge triggered by the primary, vertical fast breakdown that generates the NBE.

To better understand the multiple-pulse BLUEs, we simulated the propagation of their optical emissions within the thundercloud with both an analytical diffusion model and a Monte Carlo model (Li et al., 2020) (see Methodology in Supplemental Material for further details). Table 2 lists the inferred parameters of the multiple-pulse BLUEs. The estimated depths L (relative to the cloud top) of the BLUEs are derived by the analytical diffusion model based on the 337-nm photometer signals of MMIA, assumimg a cloud particle radius $r = 20\,\mu\text{m}$ and droplet number density $N_d = 10^8\,\text{m}^{-3} to 3\times10^8\,\text{m}^{-3}$. The altitudes H of the NBEs are evaluated based on the ground-based VLF/LF radio signals by using the simplified ray-theory method (Smith et al., 1999, 2004), which involves an uncertainty of about ±1 km (Li et al., 2020).

We see in Table 2 that the positive NBEs are located at relatively high altitudes with $H = 16\,\text{km} to 18\,\text{km}$, which are above the median heights of the majority of positive NBEs (about 13 km) reported in the literature (Smith et al., 2004; Wu et al., 2014; F. Liu, Zhu, et al., 2021). This suggests that the occurrence of multi-pulsed BLUE events may be related to the rare occurrence of high-altitude positive NBEs (Wu et al., 2014). As shown in Table 2, our modeling indicates that the subsequent BLUE pulses are located at similar or slightly higher altitudes than the primary BLUEs, with a depth of $L = 1\,\mathrm{km} to 3\,\mathrm{km}$ measured from the cloud top. This low depth explains why MMIA not only detects the primary BLUEs but also their subsequent BLUE pluses. The optical energy in the 337-nm band emitted by fast breakdown of the primary NBE is about 10^3 J, which involves around 10^8 streamer branching events evaluated as discussed by Li et al. (2021). The ratio of the irradiances and the streamer branches is expected to have a roughly linear relationship, thus the secondary BLUEs involve about 5×10^7 streamer breaching events.

We can shed some light into what differentiates multiple-pulse from single-pulse BLUEs by looking at the electrical currents of the fast breakdown where they originate. We estimated the current moments (M_i) of all the 16 BLUEs with sufficient data in the investigated thunderstorm, including the 8 multiple-pulse BLUEs and the 8 single-pulse BLUEs. Starting from the azimuthal magnetic field component, B_ϕ, we solved the inverse convolution problem using the Uman's equation (Uman et al., 1975) shown in (see Methodology and Figure S10 in the Supplemental Material for further details). Figure 4 shows a linear relationship between the amplitude of the azimuthal magnetic field component B_ϕ and the estimated current moment M_i. Despite one outlier far from the other multiple-pulse BLUEs with ID 7, all the single-pulse and multiple-pulse BLUEs are well separated into two clusters. The primary BLUEs of the multiple-pulse BLUEs have relatively weaker current moments and amplitudes than those corresponding to the single-pulse BLUEs. This is reminiscent of initiation-type NBEs, which also have weaker source currents. We emphasize however that all the multiple-pulse NBEs that we analyzed are isolated NBEs, separated from any IC or CG lightning discharges detected by either GLD360 or the 777.4-nm band of MMIA within at least 100 ms. They are also located at relatively high altitudes nearby cloud tops, unlike the INBEs normally located deeply inside the thundercloud (Smith et al., 2004; Wu et al., 2014).

4 Discussion and conclusions

Our results suggest that a fraction of so-called isolated NBEs, which do not initiate leader activity and are therefore not the starting event of a lightning flash, nevertheless trigger subsequent fast breakdown activity. We now discuss some implications of these findings.

Turning first to the thunderstorm environment that surrounds the analyzed multiple-pulse BLUEs, we notice from the lightning distribution in Figure 1 that the rate of negative CGs exceeds that of positive ones by about a factor three, which suggests that the thunderstorm has a dipole-like electrical structure with the positive charge above the negative charge (Wilson, 1956). However, the charge structures can be more complex in the convective region of the thunderstorm (Stolzenburg et al., 1998). Both IC and CG flash rates vary dramatically during the time interval when the BLUEs occurred.

The negative CG rate decreases sharply as the rate of the positive ICs increases, and later the rates of all ICs and CGs start to increase. The dramatic change of the lightning rates suggests that the lightning discharges are produced inside a thunderstorm with deep convective updrafts (Wiens et al., 2005; Petersen & Rutledge, 1998). The ring structures shown in Figure S5 and S7 further illustrate that there is a cloud turret extending above the cloud top surface during the occurrence interval of the BLUEs (Luque et al., 2020). One hypothesis for this is that the positive NBEs are produced between the positive charge lifted to relatively high altitude by the strong updraft and the negative screening charge layer which lies close to the overshooting region of the cloud (MacGorman et al., 2017).

Our results are connected to the problem of lightning initiation and the nature of fast breakdown. If our interpretation is correct, there is an intermediate class of fast breakdown discharges between those that are fully isolated and those that initiate a leader. This would be the class of breakdowns that trigger subsequent discharges which do not promote to leaders. It is unclear whether these discharges, with a primarily horizontal orientation and associated with faint radio pulses, are similar to the primarily vertical fast breakdown events described previously in the literature (Rison et al., 2016; Tilles et al., 2019; Lyu et al., 2019; N. Y. Liu & Dwyer, 2020; Huang et al., 2021). It is also unknown whether NBE-initiated leaders are initiated by horizontal fast breakdown. These questions should be addressed by future research.

Acknowledgments

The authors would like to thank Dr. Mohd Riduan Ahmad at Universiti Teknikal Malaysia Melaka (UTEM) for his cooperation on the VLF/LF sferics at Melaka station. This work was supported by the European Research Council (ERC) under the European Union H2020 programme/ERC grant agreement 681257. It also received funding from the European Union Horizon 2020 research and innovation programme under the Marie Sklodowska-Curie grant agreement SAINT 722337. Additionally, this work was supported by the Spanish Ministry of Science and Innovation, MINECO, under the project PID2019-109269RB-C43 and FEDER program. D.L., A.L. and F.J.G.V. acknowledge financial support from the State Agency for Research of the Spanish MCIU through the "Center of Excellence Severo Ochoa" award for the Instituto de Astrofísica de Andalucía (SEV-2017-0709).

Open Research

The Modular Multispectral Imaging Array (MMIA) level 1 data is proprietary and not currently available for public release. Interested parties should direct their request to the ASIM Facility Science Team (FST). ASIM data request can be submitted through: https://asdc.space.dtu.dk by sending a message to the electronic address asdc@space.dtu.dk. The Himawari-8 gridded data in this study is public to the registered users and supplied by the P-Tree System, Japan Aerospace Exploration Agency (JAXA)/Earth Observation Research Center (EORC) (`https://www.eorc.jaxa.jp/ptree/`). The data that support the findings of this study are openly available in `https://doi.org/10.5281/zenodo.6123813`. The Cloudscat Monte Carlo simulation code (Luque et al., 2020) is available at `https://github.com/aluque/CloudScat.jl`. The stanford Full-Wave Method (StanfordFWM) code (Lehtinen & Inan, 2008, 2009) is available at `https://gitlab.com/nleht/stanfordfwm/`.

References

Ahmad, M. R., Periannan, D., Sabri, M. H. M., Aziz, M. Z. A. A., Lu, G., Zhang, H., … Cooray, V. (2017). Emission heights of narrow bipolar events in a tropical storm over the Malacca Strait. In *2017 international conference on electrical engineering and computer science (icecos)* (p. 305-309). doi: https://doi.org/10.1109/ICECOS.2017.8167155

Attanasio, A., da Silva, C., & Krehbiel, P. (2021). Electrostatic conditions that produce fast breakdown in thunderstorms. *Journal of Geophysical Research: Atmospheres*, *126*(19), e2021JD034829. (e2021JD034829 2021JD034829) doi: https://doi.org/10.1029/2021JD034829

Bandara, S., Marshall, T., Karunarathne, S., Karunarathne, N., Siedlecki, R., & Stolzenburg, M. (2019). Characterizing three types of negative narrow bipolar events in thunderstorms. *Atmospheric Research*, *227*, 263-279. doi: https://doi.org/10.1016/j.atmosres.2019.05.013

Bessho, K., Date, K., Hayashi, M., Ikeda, A., Imai, T., Inoue, H., … others (2016). An introduction to Himawari-8/9—Japan's new-generation geostationary meteorological satellites. *Journal of the Meteorological Society of Japan. Ser. II*, *94*(2), 151–183. doi: https://doi.org/10.2151/jmsj.2016-009

Chanrion, O., Neubert, T., Rasmussen, I. L., Stoltze, C., Tcherniak, D., Jessen, N. C., … others (2019). The modular multispectral imaging array (MMIA) of the ASIM payload on the international space station. *Space Science Reviews*, *215*(4), 1–25. doi: https://doi.org/10.1007/s11214-019-0593-y

Huang, A., Cummer, S. A., & Pu, Y. (2021). Lightning Initiation from Fast Negative Breakdown is Led by Positive Polarity Dominated Streamers. *Geophysical Research Letters*, *48*, e2020GL091553. doi: 10.1029/2020GL091553

Kolmašová, I., Santolík, O., Defer, E., Rison, W., Coquillat, S., Pedeboy, S., … Pont, V. (2018, February). Lightning initiation: Strong pulses of VHF radiation accompany preliminary breakdown. *Scientific Reports*, *8*, 3650. doi: https://doi.org/10.1038/s41598-018-21972-z

Kostinskiy, A. Y., Marshall, T. C., & Stolzenburg, M. (2020). The mechanism of the origin and development of lightning from initiating event to initial breakdown pulses (v.2). *Journal of Geophysical Research: Atmospheres*, *125*(22), e2020JD033191. doi: https://doi.org/10.1029/2020JD033191

Lehtinen, N. G., & Inan, U. S. (2008). Radiation of elf/vlf waves by harmonically varying currents into a stratified ionosphere with application to radiation by a modulated electrojet. *Journal of Geophysical Research: Space Physics*, *113*(A6), A06301. doi: https://doi.org/10.1029/2007JA012911

Lehtinen, N. G., & Inan, U. S. (2009). Full-wave modeling of transionospheric propagation of vlf waves. *Geophysical Research Letters*, *36*(3), L03104. doi: https://doi.org/10.1029/2008GL036535

Li, D., Liu, F., Pérez-Invernón, F. J., Lu, G., Qin, Z., Zhu, B., & Luque, A. (2020). On the accuracy of ray-theory methods to determine the altitudes of intracloud electric discharges and ionospheric reflections: Application to narrow bipolar events. *Journal of Geophysical Research: Atmospheres*, *125*(9), e2019JD032099. doi: https://doi.org/10.1029/2019JD032099

Li, D., Luque, A., Gordillo-Vázquez, F. J., Liu, F., Lu, G., Neubert, T., … Reglero, V. (2021). Blue Flashes as Counterparts to Narrow Bipolar Events: The Optical Signal of Shallow In-Cloud Discharges. *Journal of Geophysical Research: Atmospheres*, *126*(13), e2021JD035013. doi: 10.1029/2021JD035013

Liu, F., Lu, G., Neubert, T., Lei, J., Chanrion, O., Østgaard, N., … Zhu, B. (2021). Optical emissions associated with narrow bipolar events from thunderstorm clouds penetrating into the stratosphere. *Nature Communications*, *12*(6631). doi: https://doi.org/10.1038/s41467-021-26914-4

Liu, F., Zhu, B., Lu, G., Lei, J., Shao, J., Chen, Y., … Zhou, H. (2021). Meteorological and electrical conditions of two mid-latitude thunderstorms producing blue discharges. *Journal of Geophysical Research: Atmospheres*, *126*(8), e2020JD033648. doi: https://doi.org/10.1029/2020JD033648

Liu, N., Dwyer, J. R., Tilles, J. N., Stanley, M. A., Krehbiel, P. R., Rison, W., … Wilson, J. G. (2019). Understanding the radio spectrum of thunderstorm narrow bipolar events. *Journal of Geophysical Research: Atmospheres*, *124*(17-18), 10134-10153. doi: https://doi.org/10.1029/2019JD030439

Liu, N. Y., & Dwyer, J. R. (2020). Thunderstorm high-frequency radio bursts with weak low-frequency radiation. *Geophysical Research Letters*, *47*(23), e2020GL090325. doi: https://doi.org/10.1029/2020GL090325

Luque, A., Gordillo-Vázquez, F. J., Li, D., Malagón-Romero, A., Pérez-Invernón, F. J., Schmalzried, A., … Østgaard, N. (2020). Modeling lightning observations from space-based platforms (Cloudscat.jl 1.0). *Geoscientific Model Development*, *13*(11), 5549–5566. doi: https://doi.org/10.5194/gmd-13-5549-2020

Lyu, F., Cummer, S. A., Qin, Z., & Chen, M. (2019). Lightning initiation processes imaged with very high frequency broadband interferometry. *Journal of Geophysical Research: Atmospheres*, *124*(6), 2994-3004. doi: https://doi.org/10.1029/2018JD029817

MacGorman, D. R., Elliott, M. S., & DiGangi, E. (2017). Electrical discharges in the overshooting tops of thunderstorms. *Journal of Geophysical Research: Atmospheres*, *122*(5), 2929-2957. doi: https://doi.org/10.1002/2016JD025933

Neubert, T., Østgaard, N., Reglero, V., Blanc, E., Chanrion, O., Oxborrow, C. A., … Bhanderi, D. D. (2019). The ASIM mission on the international space station. *Space Science Reviews*, *215*(2), 1–17. doi: https://doi.org/10.1007/s11214-019-0592-z

Nijdam, S., Teunissen, J., & Ebert, U. (2020, nov). The physics of streamer discharge phenomena. *Plasma Sources Science and Technology*, *29*(10), 103001. doi: 10.1088/1361-6595/abaa05

Petersen, W. A., & Rutledge, S. A. (1998). On the relationship between cloud-to-ground lightning and convective rainfall. *Journal of Geophysical Research: Atmospheres*, *103*(D12), 14025-14040. doi: https://doi.org/10.1029/97JD02064

Rison, W., Krehbiel, P. R., Stock, M. G., Edens, H. E., Shao, X.-M., Thomas, R. J., … Zhang, Y. (2016). Observations of narrow bipolar events reveal how lightning is initiated in thunderstorms. *Nature communications*, *7*, 10721. doi: 10.1038/ncomms10721(2016)

Said, R., & Murphy, M. (2016). GLD360 upgrade: Performance analysis and applications. In *24th international lightning detection conference.*

Smith, D. A., Heavner, M. J., Jacobson, A. R., Shao, X. M., Massey, R. S., Sheldon, R. J., & Wiens, K. C. (2004). A method for determining intracloud lightning and ionospheric heights from VLF/LF electric field records. *Radio Science*, *39*(1), RS1010. doi: https://doi.org/10.1029/2002RS002790

Smith, D. A., Shao, X. M., Holden, D. N., Rhodes, C. T., Brook, M., Krehbiel, P. R., … Thomas, R. J. (1999). A distinct class of isolated intracloud lightning discharges and their associated radio emissions. *Journal of Geophysical Research: Atmospheres*, *104*(D4), 4189-4212. doi: https://doi.org/10.1029/1998JD200045

Soler, S., Gordillo-Vázquez, F. J., Pérez-Invernón, F. J., Luque, A., Li, D., Neubert, T., … Østgaard, N. (2021). Global frequency and geographical distribution of nighttime streamer corona discharges (blues) in thunderclouds. *Geophysical Research Letters*, *48*(18), e2021GL094657. doi: https://doi.org/10.1029/2021GL094657

Soler, S., Pérez-Invernón, F. J., Gordillo-Vázquez, F. J., Luque, A., Li, D., Malagón-Romero, A., … Østgaard, N. (2020). Blue optical observations of narrow bipolar events by ASIM suggest corona streamer activity in thunderstorms. *Journal of Geophysical Research: Atmospheres*, *125*(16), e2020JD032708. doi: 10.1029/2020JD032708

Sterpka, C., Dwyer, J., Liu, N., Hare, B. M., Scholten, O., Buitink, S., … Nelles, A. (2021). The spontaneous nature of lightning initiation revealed. *Geophysical Research Letters*, *48*(23), e2021GL095511. (e2021GL095511 2021GL095511) doi: https://doi.org/10.1029/2021GL095511

Stolzenburg, M., Rust, W. D., & Marshall, T. C. (1998). Electrical structure in thunderstorm convective regions: 3. synthesis. *Journal of Geophysical Research: Atmospheres*, *103*(D12), 14097-14108. doi: https://doi.org/10.1029/97JD03545

Tilles, J. N., Liu, N., Stanley, M. A., Krehbiel, P. R., Rison, W., Stock, M. G., … Wilson, J. (2019). Fast negative breakdown in thunderstorms. *Nature communications*, *10*(1), 1–12.

Uman, M. A., McLain, D. K., & Krider, E. P. (1975). The electromagnetic radiation from a finite antenna. *American Journal of Physics*, *43*(1), 33-38. doi: 10.1119/1.10027

Wiens, K. C., Rutledge, S. A., & Tessendorf, S. A. (2005). The 29 june 2000 supercell observed during steps. part ii: Lightning and charge structure. *Journal of the Atmospheric Sciences*, *62*(12), 4151 - 4177. doi: 10.1175/JAS3615.1

Wilson, C. T. R. (1956). A Theory of Thundercloud Electricity. *Proceedings of the Royal Society of London. Series A, Mathematical and Physical Sciences*, *236*(1206), 297–317. Retrieved from `http://www.jstor.org/stable/99960` doi: 10.1098/rspa.1956.0137

Wu, T., Yoshida, S., Akiyama, Y., Stock, M., Ushio, T., & Kawasaki, Z. (2015). Preliminary breakdown of intracloud lightning: Initiation altitude, propagation speed, pulse train characteristics, and step length estimation. *Journal of Geophysical Research: Atmospheres*, *120*(18), 9071-9086. doi: https://doi.org/10.1002/2015JD023546

Wu, T., Yoshida, S., Ushio, T., Kawasaki, Z., & Wang, D. (2014). Lightning-initiator type of narrow bipolar events and their subsequent pulse trains. *Journal of Geophysical Research: Atmospheres*, *119*(12), 7425-7438. doi: https://doi.org/10.1002/2014JD021842

Zhang, H., Lu, G., Qie, X., Jiang, R., Fan, Y., Tian, Y., … Feng, G. (2016). Locating narrow bipolar events with single-station measurement of low-frequency magnetic fields. *Journal of Atmospheric and Solar-Terrestrial Physics*, *143-144*, 88-101. doi: https://doi.org/10.1016/j.jastp.2016.03.009

Table list

Table 1. The detailed features of the multiple-pulse BLUEs. The detection times of MMIA have been corrected to the source time with respect to the BLUE locations.

ID	MMIA UTC time (source)	Primary BLUE			Subsequent BLUE pluses			Time difference (ms)
		Irradiance ($\mu W/m^2$)	Rise time[a] (ms)	Total time duration[b] (ms)	Irradiance ($\mu W/m^2$)	Rise time[a] (ms)	Total time duration[b] (ms)	
1	17:50:08.246	4.54	0.18	1.25	2.5	0.05	0.86	3.1
2	17:50:09.645	5.57	0.30	2.25	2.76[c]	0.58[c]	1.66[c]	6.0
3	17:50:19.447	12.42	0.17	1.53	6.08	0.14	1.61	1.7
4	17:50:24.704	10.28	0.79	6.50	3.52	0.14	3.37	9.4
5	17:50:35.617	4.54	0.59	2.45	4.54	0.68	2.64	3.3
6	17:50:43.238	8.69	0.79	3.60	4.54	0.79	3.75	2.6
7	17:50:46.157	10.81	0.06	1.93	3.01	0.22	1.15	7.3
8	17:50:55.181	3.01	0.12	1.19	3.01[c]	0.41[c]	2.55[c]	1.4

[a] Rise time is the time taken for the amplitude of a MMIA photometer signal to rise from 10% to 90%.
[b] Time duration is the time interval for the amplitude of a MMIA photometer signal to rise from 10 % and fall to 10%.
[c] The first subsequent BLUE pulse is used to evaluate the rise time and time duration since the photometer signal includes multiple pulses (see Figure S3 and S9 in Supplemental Material for details).

Table 2. The inferred features of the multiple-pulse BLUEs. The altitudes (H) are estimated using the simplified ray-theory method proposed by (Smith et al., 1999, 2004) based on the ground-based VLF/LF sferics. The depths (L) relative to cloud top boundary are evaluated by using the analytical diffusion model in equation (2) in Supplemental Material based on the 337-nm photometer signals of MMIA.

ID	Parameters			NBE				Subsequent pulses
	Distance d (km)	N_d (m^{-3})	R (µm)	337-nm optical energy (J)	Streamer branching events	Altitude H (km)	Depth L (km)	Depth L (km)
1	495	3×10^8	20	1.3×10^3	1.0×10^8	17.68	0.96	0.66
2	494	2×10^8	20	3.7×10^3	2.9×10^8	16.67	1.50	1.74[a]
3	489	1×10^8	20	6.4×10^3	5.0×10^8	17.03	1.85	1.45
4[b]	486	-	-	-	-	15.55	-	-
5[b]	486	-	-	-	-	15.55	-	-
6[b]	480	-	-	-	-	15.87	-	-
7	482	1×10^8	20	3.8×10^3	3.0×10^8	17.95	1.30	2.79
8[c]	477	-	-	-	-	17.33	-	-

[a] The first subsequent BLUE pulse is used to obtain the fitting parameters since the photometer signal includes multiple subsequent BLUE pulses (see Figure S3 in Supplemental Material for details).
[b] There is a small pulse on the rising edge of light-curve that distorted the fit process (See Figure S5, S6 and S7 in Supplemental Material for details).
[c] The photometer signal is too noisy to be fitted (See Figure S9 in Supplemental Material for details).

Figures list

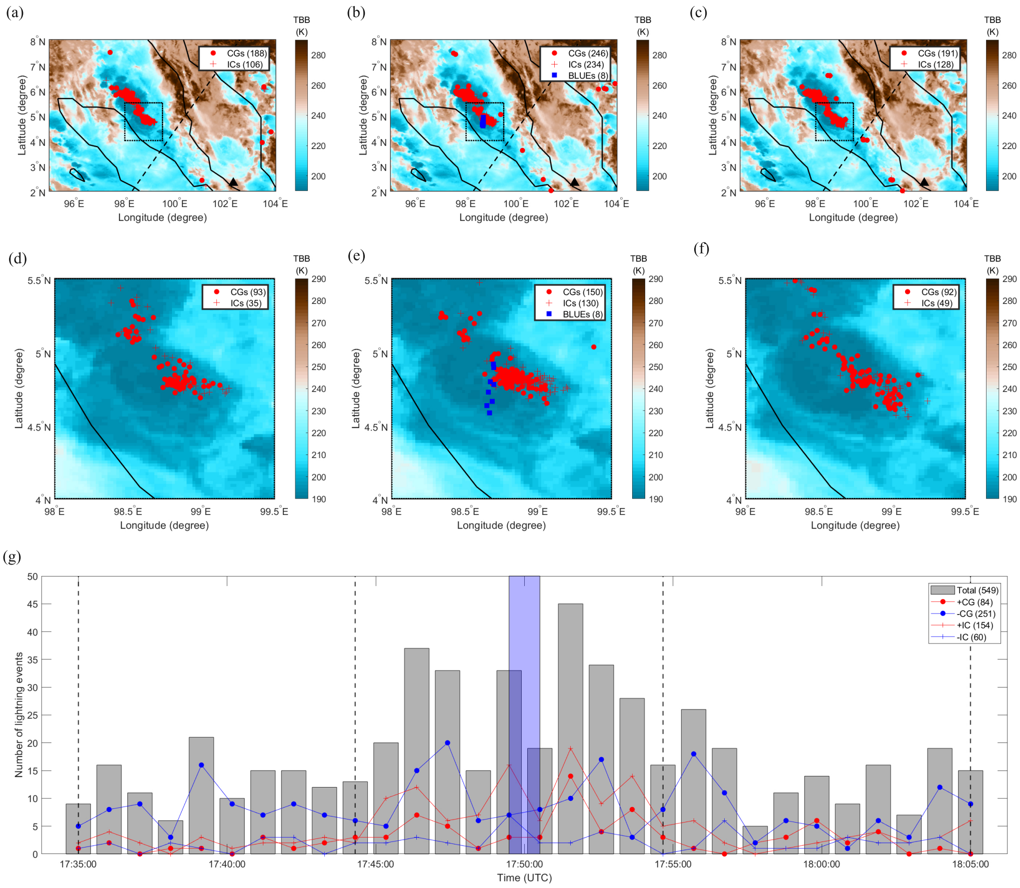

Figure 1. Distribution of the intracloud (IC)/cloud-to-ground (CG) lightning with 8 multiple-pulse BLUEs superimposed on the cloud Top Blackbody Brightness temperature (TBB, given in K) in the region of interest and the zoomed-in rectangular region, indicated with the dotted black line, per 10 minutes at time 17:40:00 UTC (a,d), 17:50:00 UTC (b,e), and 18:00:00 UTC (c,f). Numbers of different types of lightning events are shown in (g): positive CGs (+CGs), negative CGs (−CGs), positive ICs (+ICs) and negative ICs (−ICs). The multiple-pulse BLUEs occurred in the time period from 17:50:00 to 17:51:00 UTC marked in blue shaded region in (g). The ground-based VLF/LF sensor at Malaysia is shown as a black triangle in panels (a, b, c). The footprints of ASIM are shown with a black dashed line.

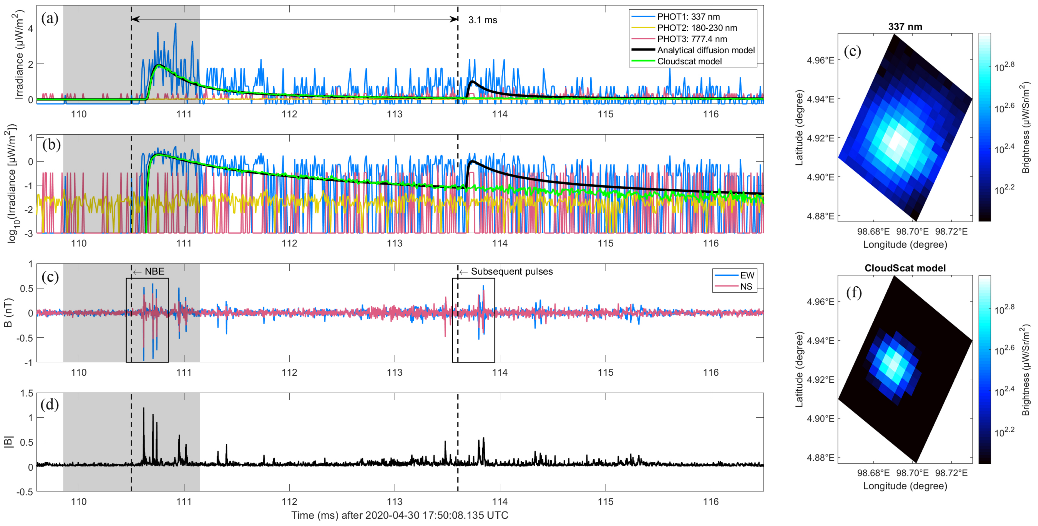

Figure 2. Comparison between MMIA photometer irradiance (blue: 337 nm, yellow: 180-230 nm and red: 777.4 nm) and the modeling results of the analytical diffusion model (black) and Cloudscat model (green) on a linear (a) and logarithmic (b) scale, shown together with the North-south and East-west magnetic field components $B_{\mathbf{NS}}$ and $B_{\mathbf{EW}}$ (c) and its norm $|B| = \sqrt{B_{\mathbf{NS}}^2 + B_{\mathbf{EW}}^2}$ (d), recorded at the ground-based VLF/LF sensor nearby Malaysia for event 1. Also shown: the image detected by the 337-nm filtered camera of MMIA (e) and the simulated image of the Cloudscat model (f). The start time (corrected to the source time with respect to the locations) for NBE and its subsequent pulses is marked with the dashed black line, within the time difference 3.1 ms with ±0.65 ms uncertainty (gray shadowed region).

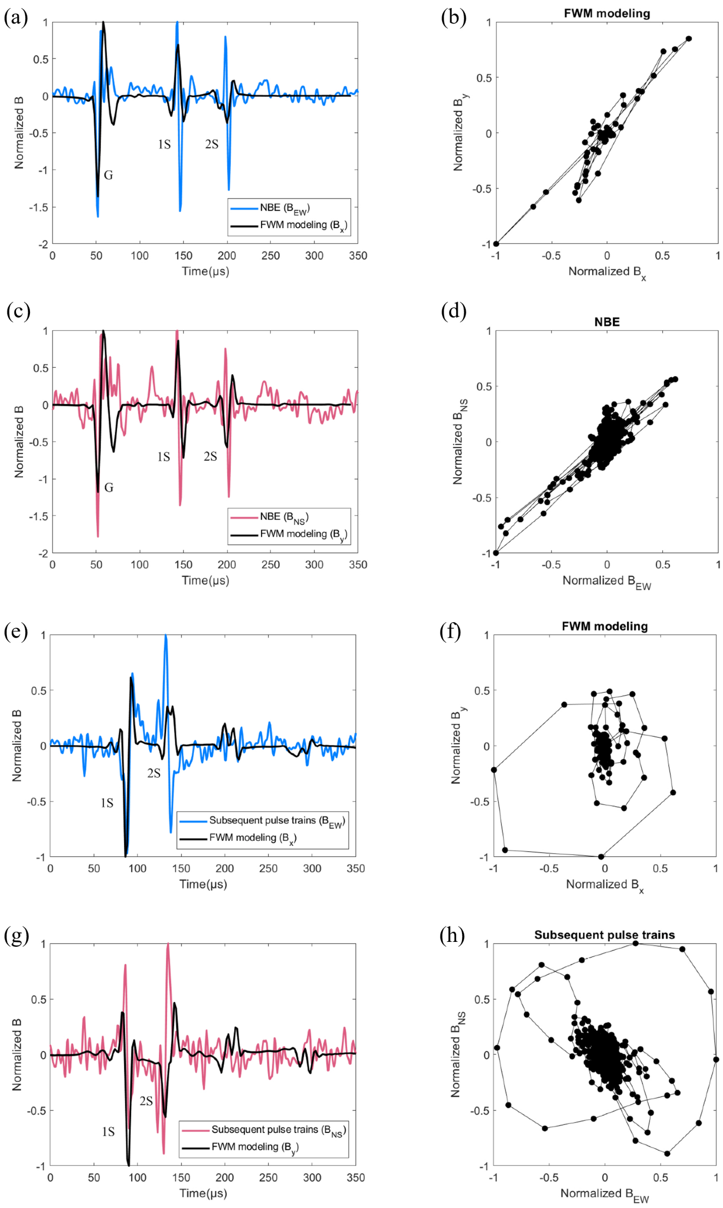

Figure 3. Comparison of normalized magnetic field components between the simulation and observation corresponding to the NBE(a,b,c,d) and the subsequent pulses (e,f,g,h) of multiple-pulse BLUE for event 1 (see the black rectangle with the NBE and subsequent pulses labels marked in the figure 2(c)). The magnetic field components of B_x and B_y are calculated by the FWM modeling and the North-South and East-West magnetic field components of $B_{\mathbf{EW}}$ and $B_{\mathbf{NS}}$ are measured by the ground-based VLF/LF sensor at Malaysia. The correlation between the different components of the simulated magnetic field (B_x and B_y) and the measured magnetic field components ($B_{\mathbf{EW}}$ and $B_{\mathbf{NS}}$) for both NBE (b,d) and the subsequent pulses (f,h) are also shown in the figure. The ground wave and two ionospheric reflected sky waves marked as G, 1S, and 2S.

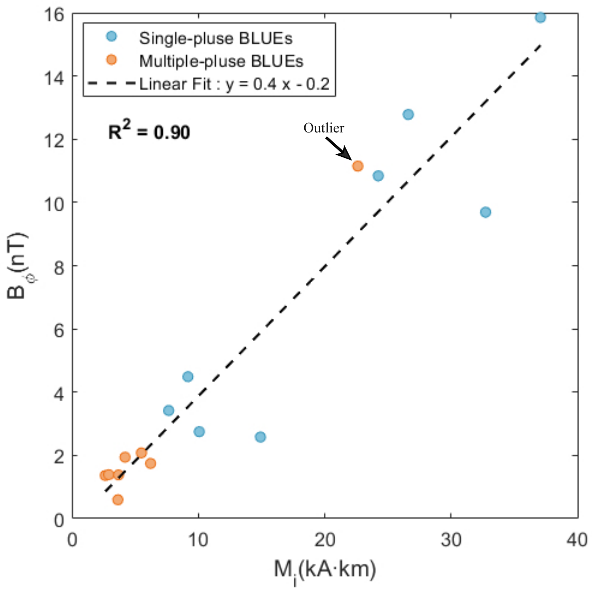

Figure 4. Correlation between the amplitude of the azimuthal magnetic field component B_ϕ and the inferred current moment M_i for all the detected BLUEs (8 single-pulse BLUEs (blue dots) and 8 multiple-pulse BLUEs analyzed in the paper (red dots)). The outlier of the multiple-pulse BLUEs corresponds to the event with ID 7 in Figure S8 in Supplemental Materials.

Supplemental Material for "Multi-pulse corona discharges in thunderclouds observed in optical and radio bands"

Dongshuai Li[1], Alejandro Luque[1], Nikolai G. Lehtinen[2], F. J. Gordillo-Vázquez[1], Torsten Neubert[3], Gaopeng Lu[4], Olivier Chanrion[3], Hongbo Zhang[5], Nikolai Østgaard[2], Víctor Reglero[6]

[1]Instituto de Astrofísica de Andalucía (IAA), CSIC, Granada, Spain.

[2]Birkeland Centre for Space Science, Department of Physics and Technology, University of Bergen, Bergen, Norway.

[3]National Space Institute, Technical University of Denmark (DTU Space), Kongens Lyngby, Denmark.

[4]CAS Key Laboratory of Geospace Environment, University of Science and Technology of China, Hefei, China.

[5]Key Laboratory of Middle Atmosphere and Global Environment Observation (LAGEO),

Institute of Atmospheric Science, Chinese Academy of Sciences, Beijing, China.

[6]Image Processing Laboratory, University of Valencia, Valencia, Spain.

Contents of this file

1. Text S1

2. Figures S1 - S19

Text S1: Methodology

MMIA observation simulation

In the simulation, we assumed the optical BLUE sources are impulsive and localized point sources inside a homogeneous isotropic cloud. The scattering and absorption processes of the photons propagating through the cloud are evaluated based on two different approaches including an analytical diffusion model and a Monte Carlo simulation (Luque et al., 2020).

We first fit the 337-nm photometer signal of MMIA to infer the depth (relative to the cloud top) L of point-like optical sources inside a homogeneous and infinite cloud. To simplify the simulation, we neglect Rayleigh scattering and background absorption by adopting a homogeneous collision rate $\nu = cN_dQ_{ext}\pi R^2$, where N_d is a droplet number density with particle radius R.

Soler et al. (2020) proposed a simplified analytical expression based on the diffusion approximation proposed by Koshak et al. (1994), named first-hitting-time model, to infer the depth (relative to the cloud top) of the point-like optical sources located deep inside the cloud. However, here we add more details by using equation (27) of Luque et al. (2020) to include Mie scattering. Mie scattering corresponding to the wavelength of 337 nm is characterized by three parameters: the scattering asymmetry parameter $g = 0.88$, the respective extinction coefficient $Q_{ext} = 2.06$ and the single-scattering albedo $\omega_0 = 0.99$ which is close to unity and describes the probability that a photon re-emits after a scattering event. These parameters are obtained by solving the Mie problem with the open source MieScatter.jl code (Wilkman, 2013; Li et al., 2020) .

The total flux per unit time of single-pulse BLUEs $F_{\text{single}}(t)$ for the analytical diffusion model is (see more details in (Luque et al., 2020)):

$$F_{\text{single}}(t) = \frac{e^{-t/\tau_A - \tau_D/t}}{\sqrt{\pi}\tau_D}(t/\tau_D)^{-3/2} \tag{1}$$

where the photon absorption time $\tau_A = \frac{1}{\nu(1-\omega_0)}$ and the characteristic time $\tau_D(t) = \frac{L^2}{4D}$ with the depth L and the diffusion coefficient $D = \frac{c^2}{\nu(1-\omega_0)}$.

The equation for multiple-pulse BLUEs, denoted as $F_{\text{multiple}}(t)$, is a sum of $F_{\text{single}}(t)$ as follows:

$$F_{\text{multiple}}(t) = \sum_{i=1}^{M} F_{\text{single}}(t) \tag{2}$$

where M is the number of the BLUE pulses used in the fitting process.

We further simulate the 337-nm photometer signal and the corresponding camera image detected by MMIA using a Monte Carlo code CloudScat.jl (Luque et al., 2020) by considering a localized optical point source inside a homogeneous cloud at an altitude that spans from 7 km to the cloud top boundary. The depth L of the optical source is derived from the analytical diffusion model with the scattering parameters listed in Table 2.

FWM simulation

We simulate the radio waveform of both NBEs and the subsequent pulse trains of the multiple-pulse BLUEs using the Stanford Full Wave Method (StanfordFWM) code of Lehtinen & Inan (2008, 2009). The source is assumed to be a vertical dipole for the NBEs and a horizontal dipole for the subesequent pluse trains with the current moment of 1 A m located at an altitude of 10 km (selected for simplicity, neglecting the small differences with the estimated source altitudes) emitting at frequencies between $10\,\text{kHz} to 100\,\text{kHz}$. The waveform of the current moment is assumed to be the bi-Gaussian function:

$$I(t) = I_0(e^{-t^2/\tau_1{}^2} - e^{-t^2/\tau_2{}^2}), \tag{3}$$

where the rise time τ_1 and the fall time τ_2. The electric current moment for the NBEs is $I_0 = [0, 0, 1]$ corresponding to a vertical dipole along z-axis. The electric current moment for subsequent pulse trains is $I_0 = [\sqrt{2}/2, \sqrt{2}/2, 0]$, i.e., represents a horizontal dipole with an angle of 45° with respect to the positive x-axis. Note that the angle of 45° here only represent an example of the cases since we don't know the exact angle of the horizontally oriented sources. The ionosphere is assumed to be horizontally stratified at altitudes between 0 km to 100 km and treated as a magnetized plasma. In order to reflect the real propagation geometry, we assumed the propagation in positive x-direction corresponding to the north component of the geomagnetic field. According to the International Geomagnetic Reference Field (IGRF) model (Alken et al., 2021), the geomagnetic field in our case has the total intensity about 42 000 nT along the positive y-axis. In the simulation, we only consider the electrons since the effect of the ions can be neglected in the lower ionosphere in the frequency range of interest. The electron density profile is obtained using the International Reference Ionosphere (IRI) model (Bilitza et al., 2014) at the location of the BLUEs at 17:50:00 UTC on April 30, 2020. The ground is assumed to be perfectly conducting without considering the effect of the ground conductivity due to the BLUEs occurred over the ocean. By following the geometry of the observation, the observed sensor at Malaysia is located at about 500 km away from the BLUEs (see figure 1(b)). After the results of the FWM modeling at different frequencies are obtained, we applied the inverse Fourier transform to calculate the time-domain waveforms of the x and y components of the magnetic field at the observation point. The comparison between the StanfordFWM results and the observation are shown in figure 3.

VLF/LF sferic simulation

We estimate the current moment $M_i(t)$ for the primary BLUE pulse of the multiple-pulse BLUEs based on the azimuthal magnetic field component B_ϕ measured by the ground-based very low frequency/low frequency (VLF/LF) sensor nearby Malaysia. In the calculation, we assumed the source as a vertical dipole located at an altitude of H away from the sensor at a distance of d (see Table 2). The ground is assumed to be perfectly conducting because the VLF waves propagation from the BLUEs occurred over the ocean. We calculate the azimuthal magnetic field component B_ϕ by using Uman's equation (Uman et al., 1975) and compare it with the observation. The source current moments can be inferred by solving the inverse convolution problem (Cummer & Inan, 2000; Cummer, 2003):

$$B(t) = \int_{-\infty}^{\infty} M_i(t) h(t-\tau) d(\tau), \tag{4}$$

where B is the measured magnetic field waveform, M_i is the source current moment and $h(t)$ is the propagation response evaluated from the modeling results of Uman's equation. In the modeling, the waveform of the source current is also assumed to be the bi-Gaussian function in equation (3). The inferred current moments M_i and the cumulative charge moments M_q of all multiple-pulse BLUEs are presented in Figure S10.

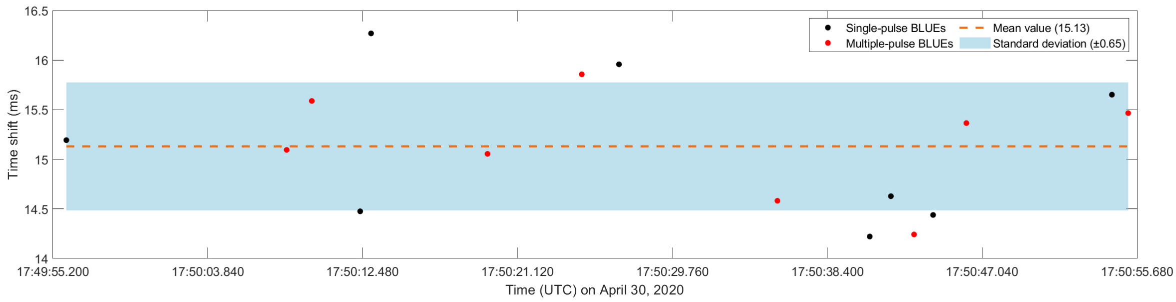

Figure S1. The systematic time shift of MMIA with respect to the ground-based VLF/LF radio signals calculated by using 16 BLUEs (8 single-pulse BLUEs (black dots) and 8 multiple-pulse BLUEs analyzed in the paper (red dots)) simultaneously detected by the 337-nm photometer and its filtered camera of MMIA and the ground-based VLF/LF sensor nearby Malaysia. The mean value of the MMIA time shift is about -15 ms with the standard deviation ± 0.65 ms.

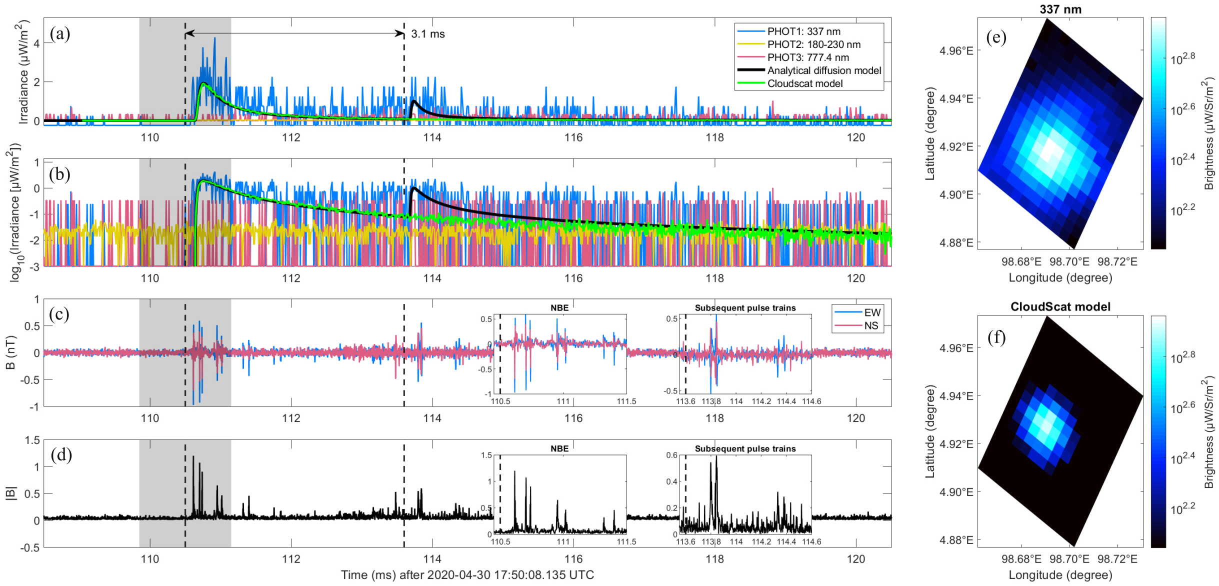

Figure S2. Comparison between MMIA photometer irradiance (blue: 337 nm, yellow: 180-230 nm and red: 777.4 nm) and the modeling results of the analytical diffusion model (black) and Cloudscat model (green) on a linear (a) and logarithmic (b) scale along with the North-south and East-west magnetic field components B_{NS} and B_{EW} (c), and their sum of the square $B_{NS^2+EW^2}$ (d) from the ground-based VLF/LF sensor nearby Malaysia for event 1. The image detected by 337-nm filtered camera of MMIA (e) and the simulated image of Cloudscat model(f). The start time (refer to source) for NBE and its subsequent pulse is marked in dashed black line within the time difference 3.1 ms with ±0.65 ms uncertainty (gray shadowed region). The inset zoom figures for both primary NBE and its subsequent pulse trains are also given in the figure.

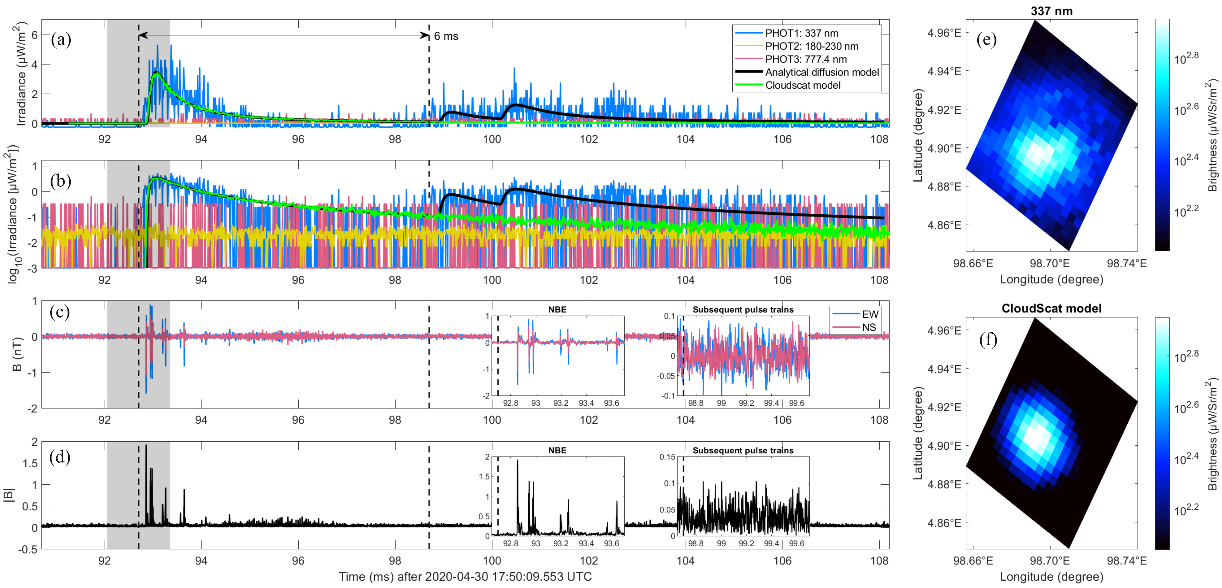

Figure S3. Similar to Figure S2, but for event 2.

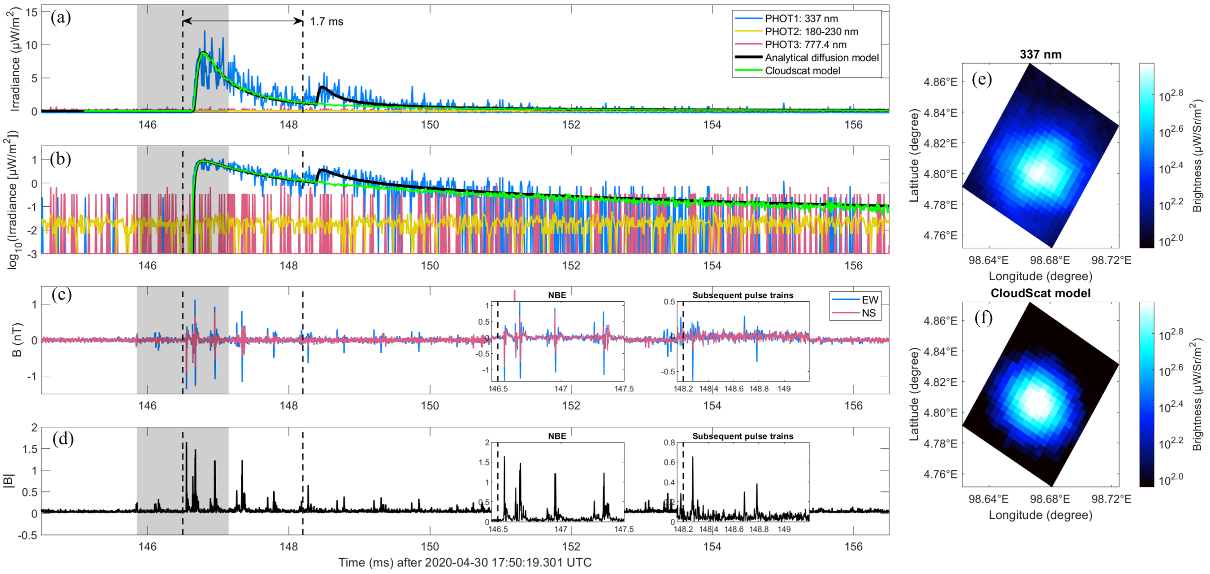

Figure S4. Similar to Figure S2, but for event 3.

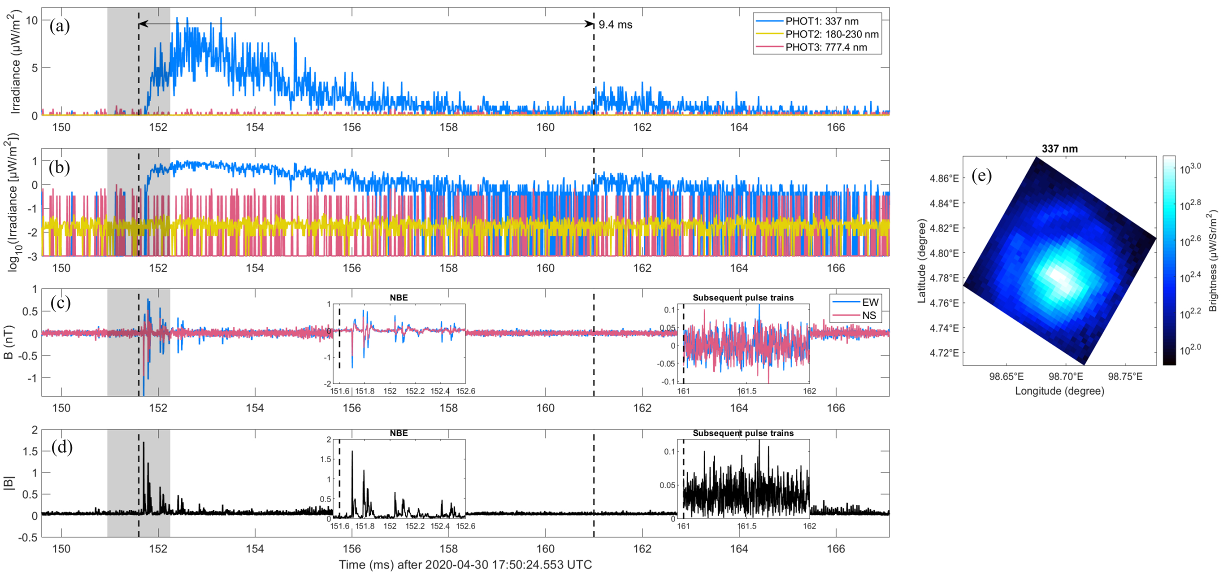

Figure S5. Photometer irradiance (blue: 337 nm, yellow: 180-230 nm and red: 777.4 nm) of MMIA on a linear (a) and logarithmic (b) scale along with the magnetic field components B_{NS}, B_{EW} (c) and their sum of the square $B_{NS^2+EW^2}$ (d) detected from the ground-based VLF/LF sensor nearby Malaysia for event 4. The image detected by 337-nm filtered cameras of MMIA (e). The start time (refer to source) for NBE and its subsequent pulse is marked in dashed black line with ±0.65 ms uncertainty (gray shadowed region). The inset zoom figures for both primary NBE and its subsequent pulse trains are also given in the figure.

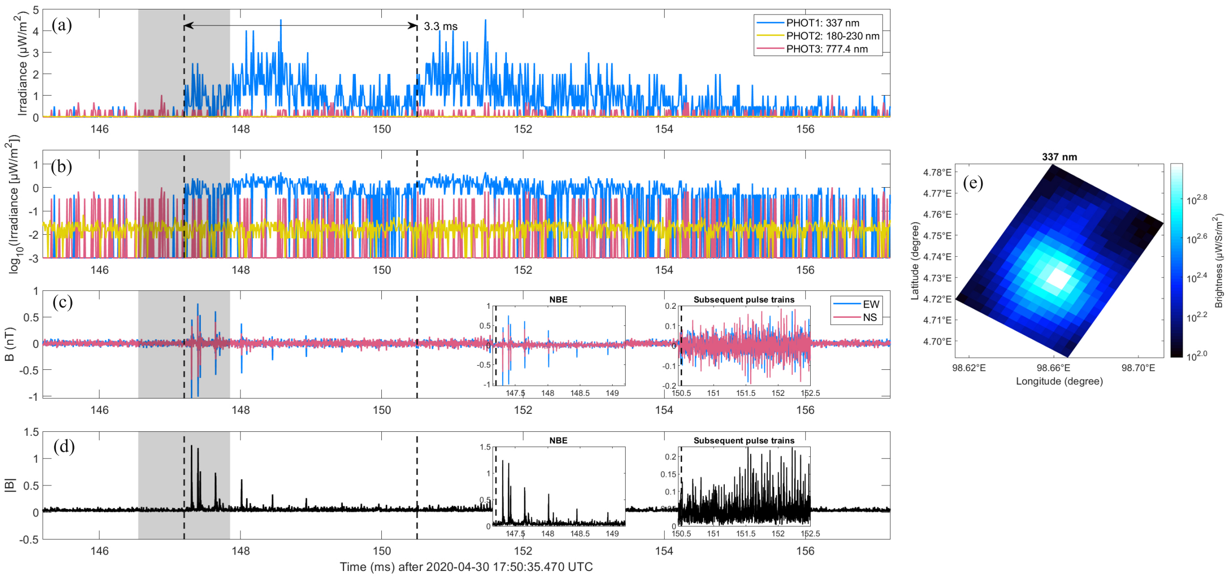

Figure S6. Similar to Figure S5, but for event 5.

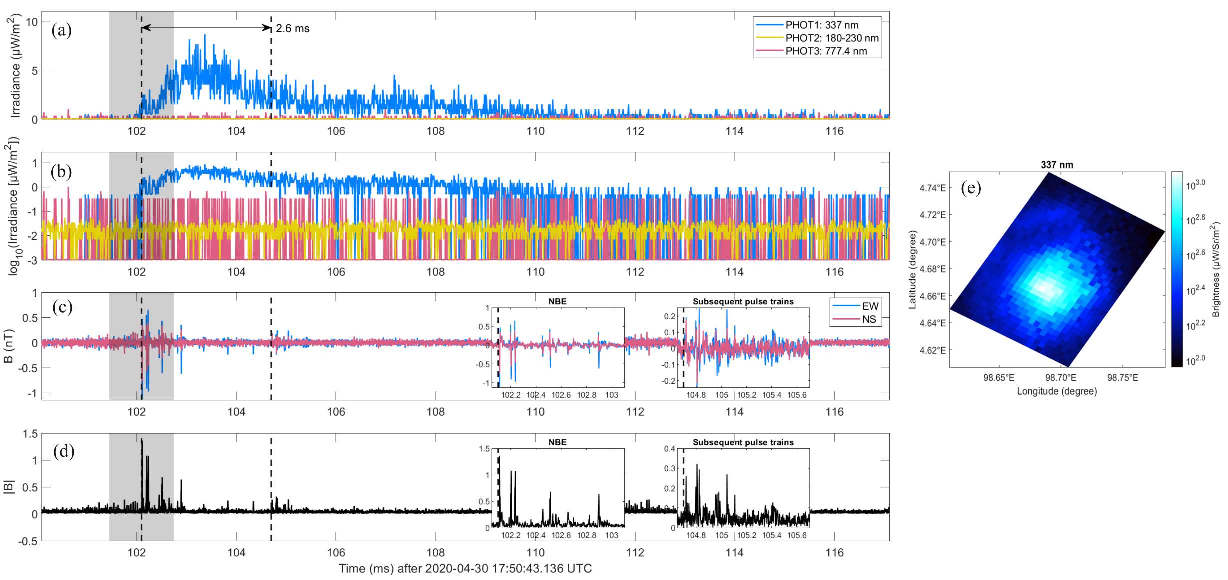

Figure S7. Similar to Figure S5, but for event 6.

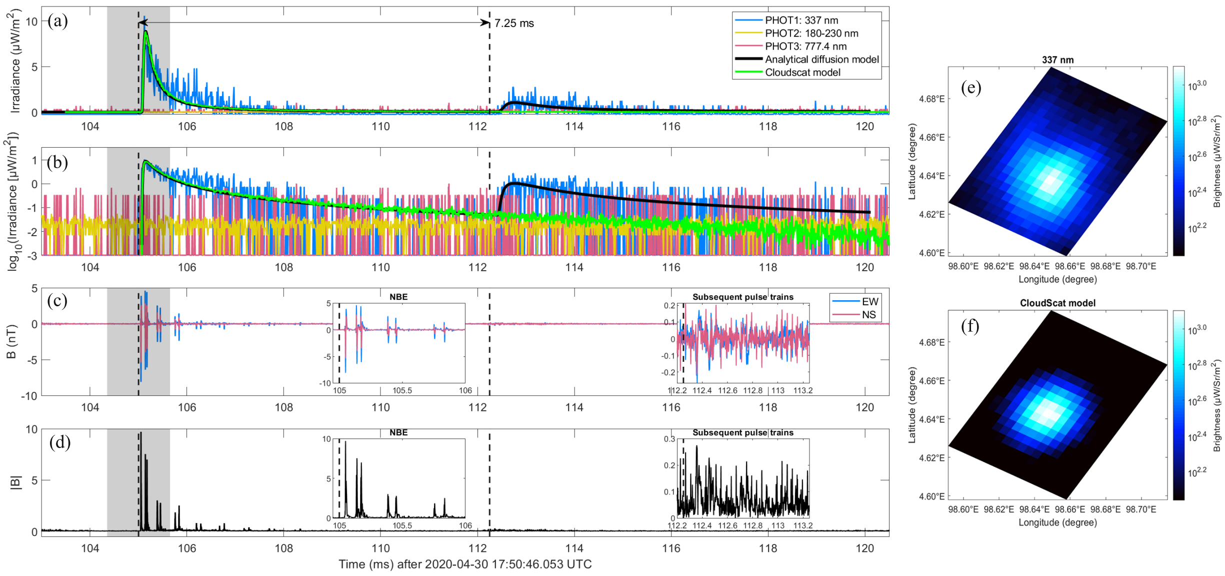

Figure S8. Similar to Figure S2, but for event 7.

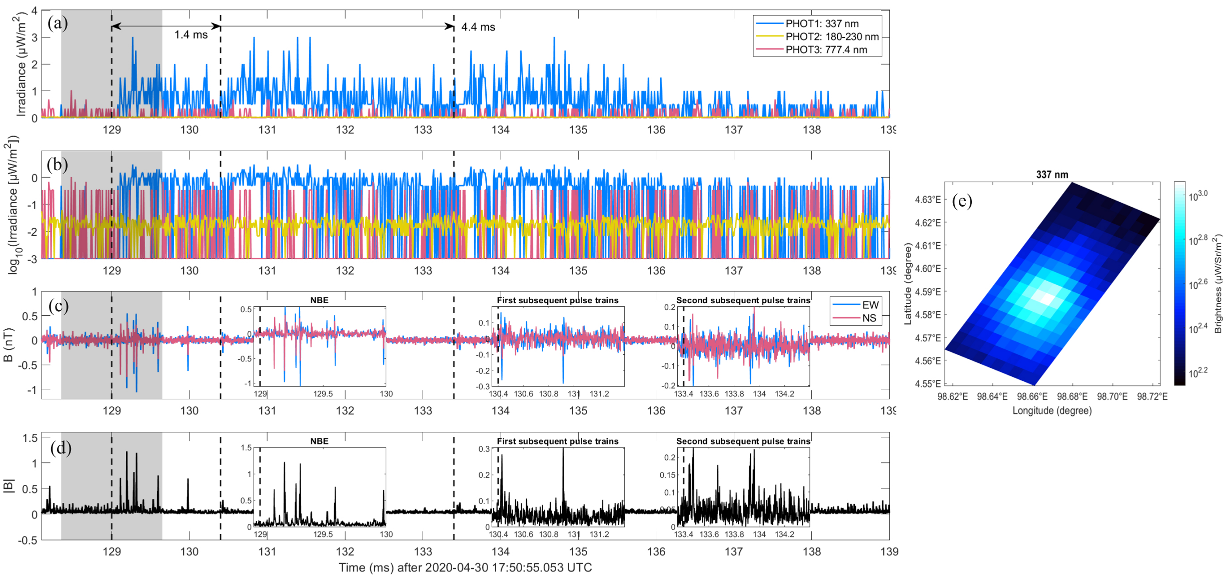

Figure S9. Similar to Figure S5, but for event 8. Note that the zoom-in of the first and second subsequent pulses trains within time difference 1.4 ms and 4.4 ms are also shown in the figure.

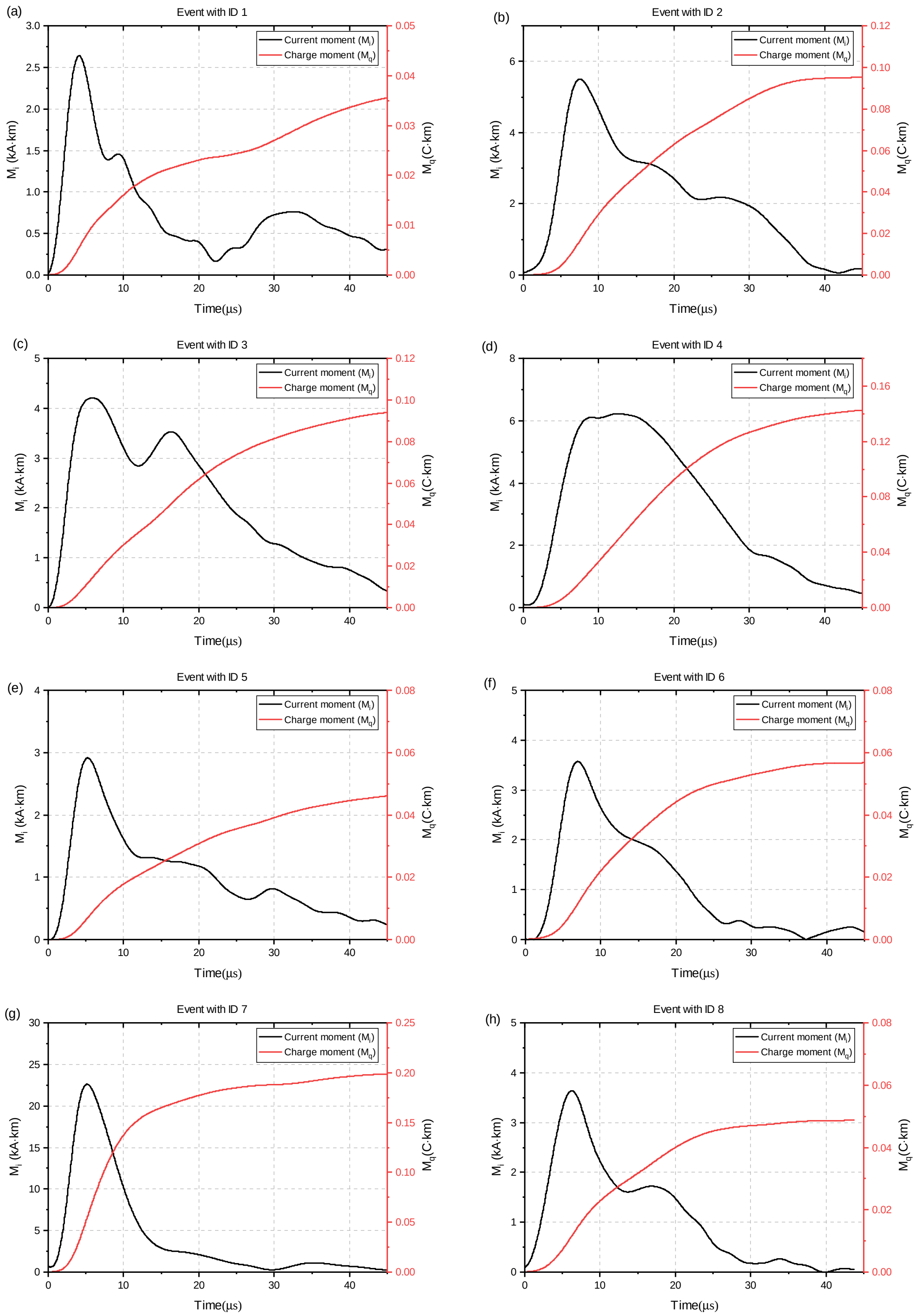

Figure S10. The evaluated current moments M_i and charge moments M_q for the primary BLUE pulse of eight multiple-pulse BLUEs listed in Table 1 based on the azimuthal magnetic field component B_ϕ measured by the ground-based very low frequency/low frequency (VLF/LF) sensor nearby Malaysia..

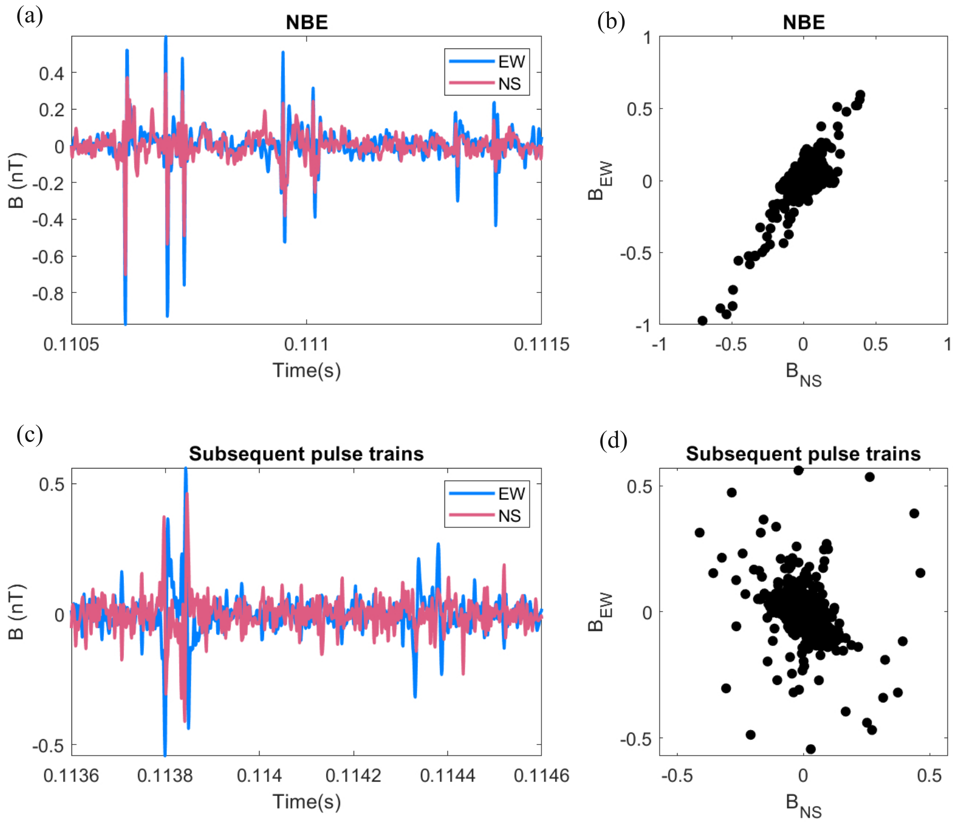

Figure S11. The waveform of the North-south and East-west magnetic field component (B_{NS} and B_{EW}) and the correlation between them for both NBE (a,b) and its subsequent pulse trains (c,d) of the multiple-pulse BLUE for event 1.

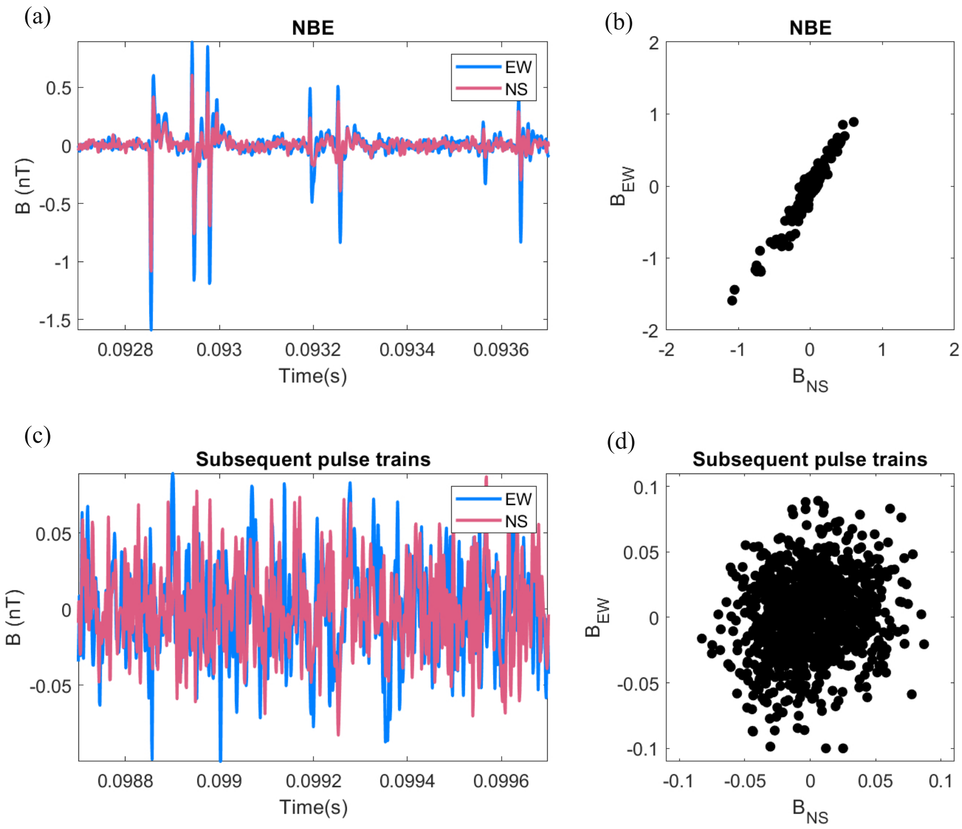

Figure S12. Similar to Figure S11, but for event 2.

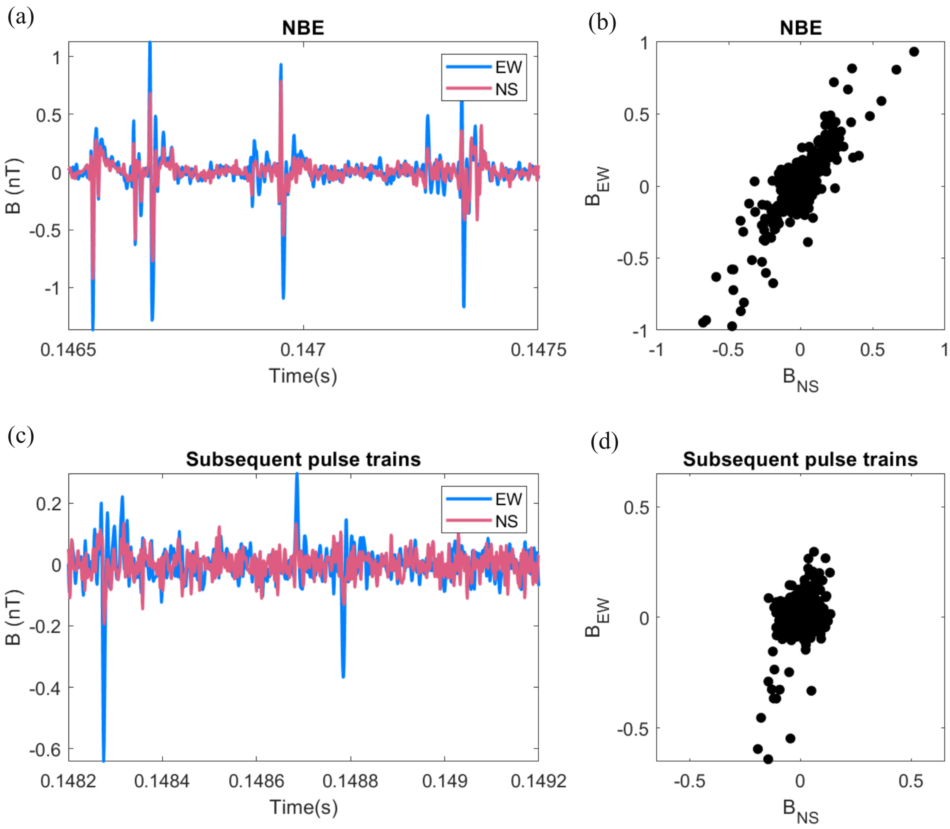

Figure S13. Similar to Figure S11, but for event 3.

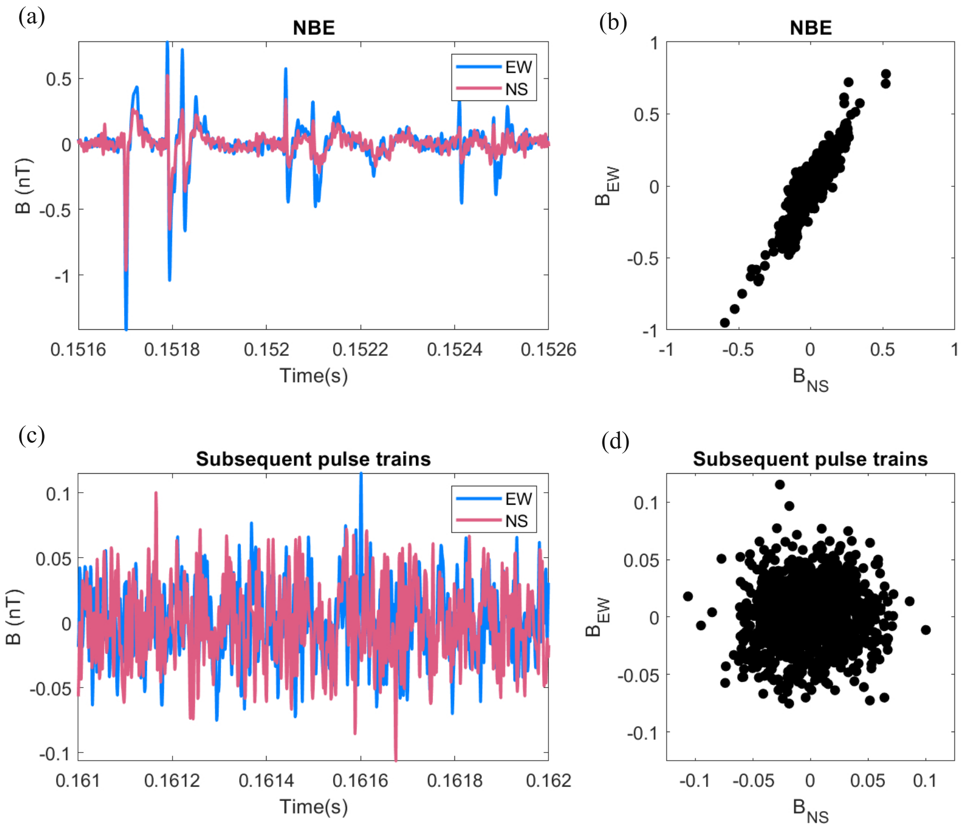

Figure S14. Similar to Figure S11, but for event 4.

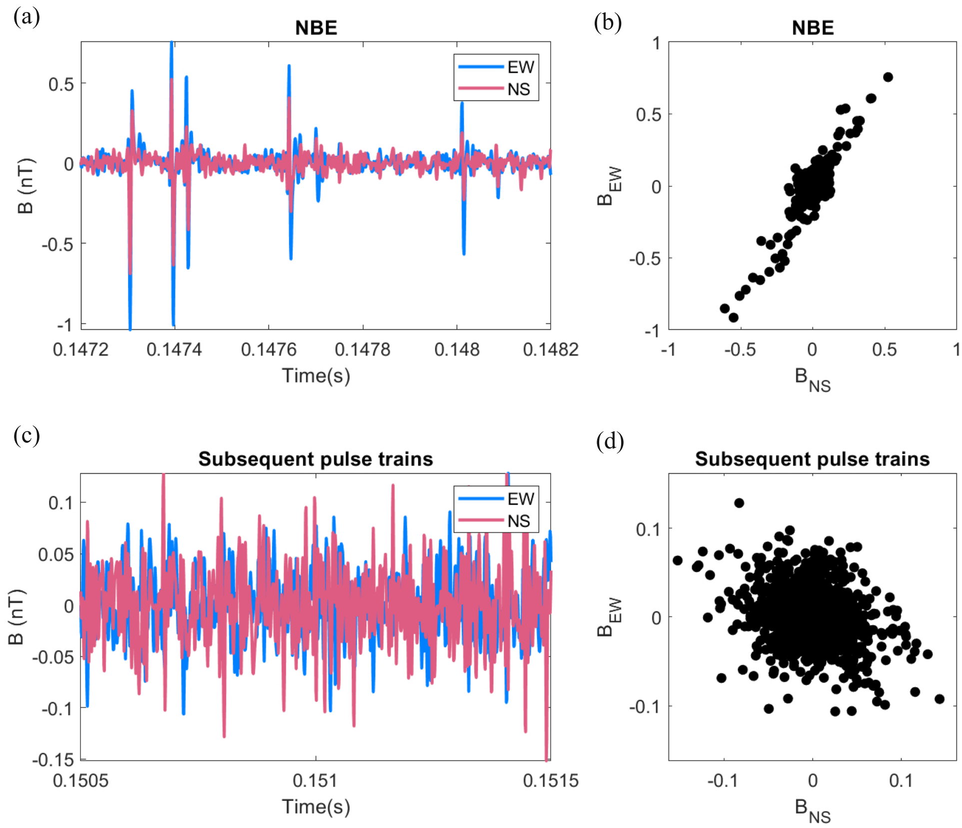

Figure S15. Similar to Figure S11, but for event 5.

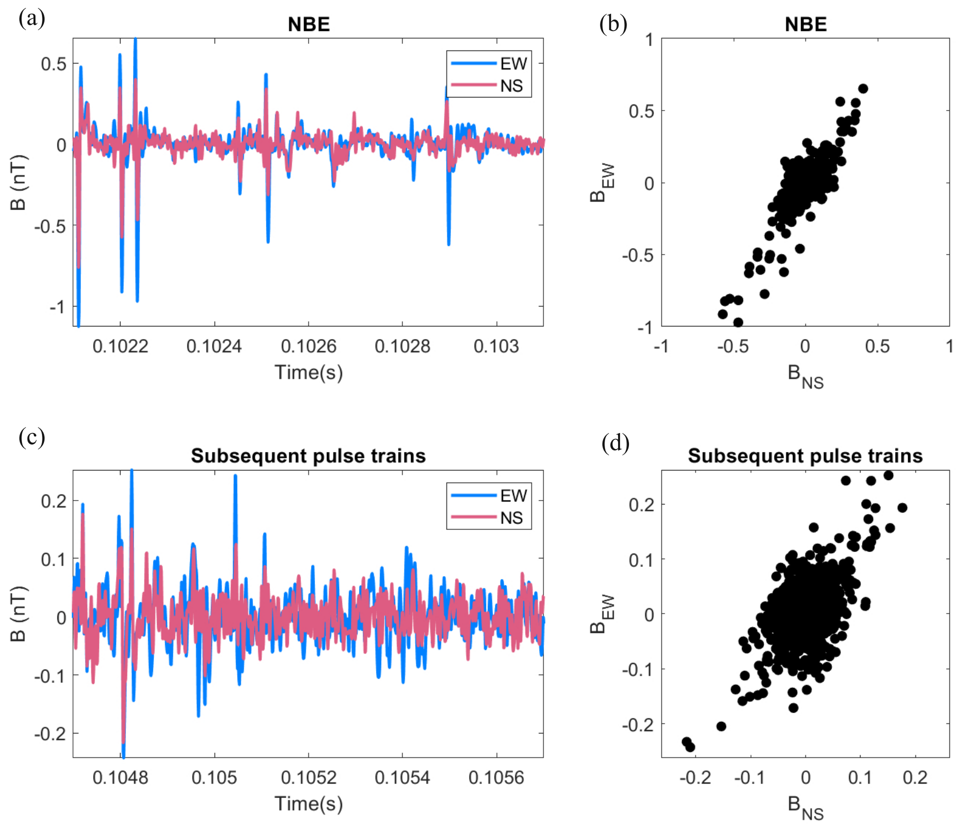

Figure S16. Similar to Figure S11, but for event 6. Note that, as shown in (d), the subsequent pulses trains show a similar linear-like pattern comparing with NBE pulses. It is due to the subsequent pulse trains for the event 6 seems like a negative NBE, however, it is too noisy to identify it through the radio signals (see (c)).

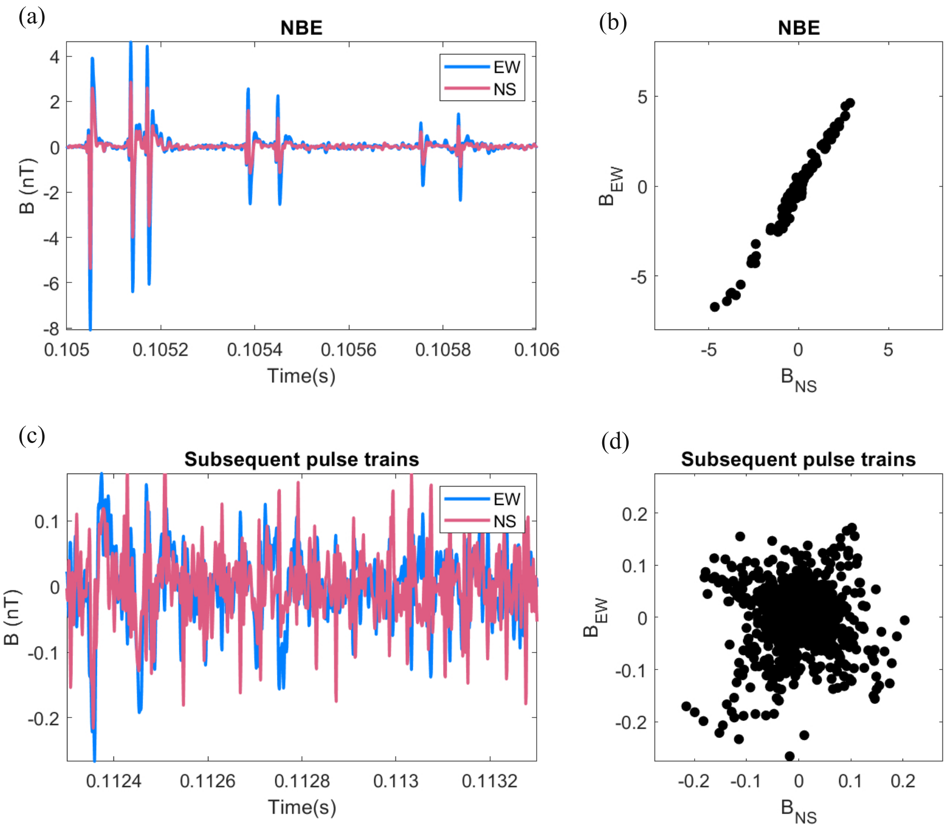

Figure S17. Similar to Figure S11, but for event 7.

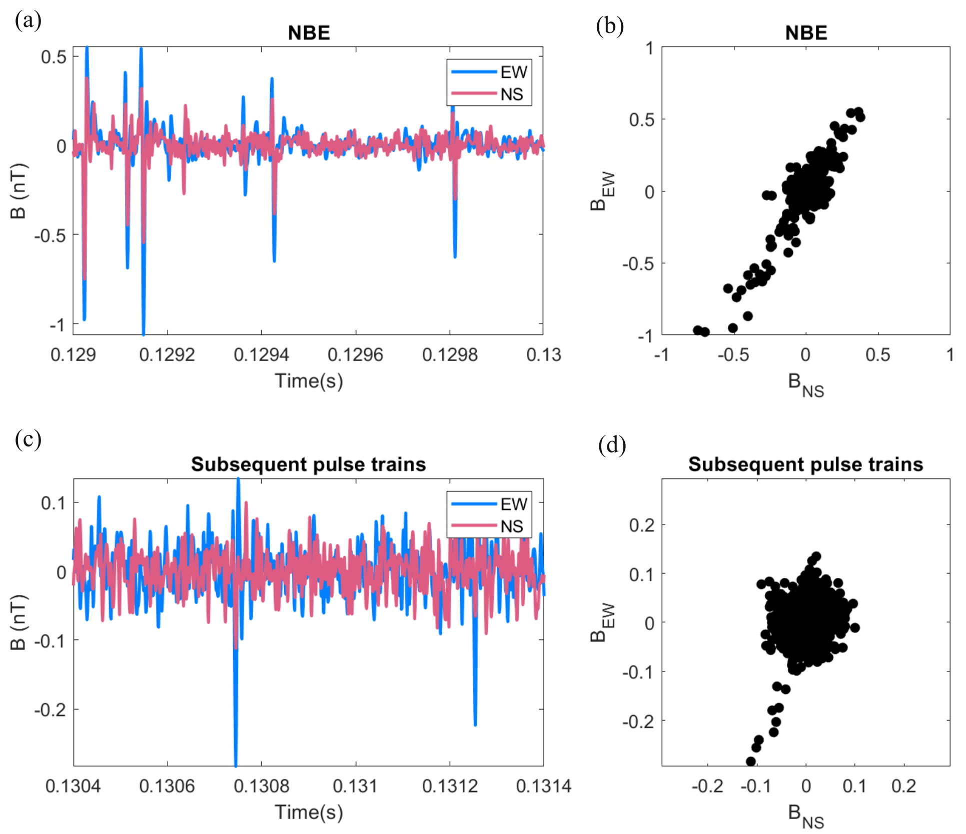

Figure S18. Similar to Figure S11, but for both NBE and its first subsequent pulse for event 8.

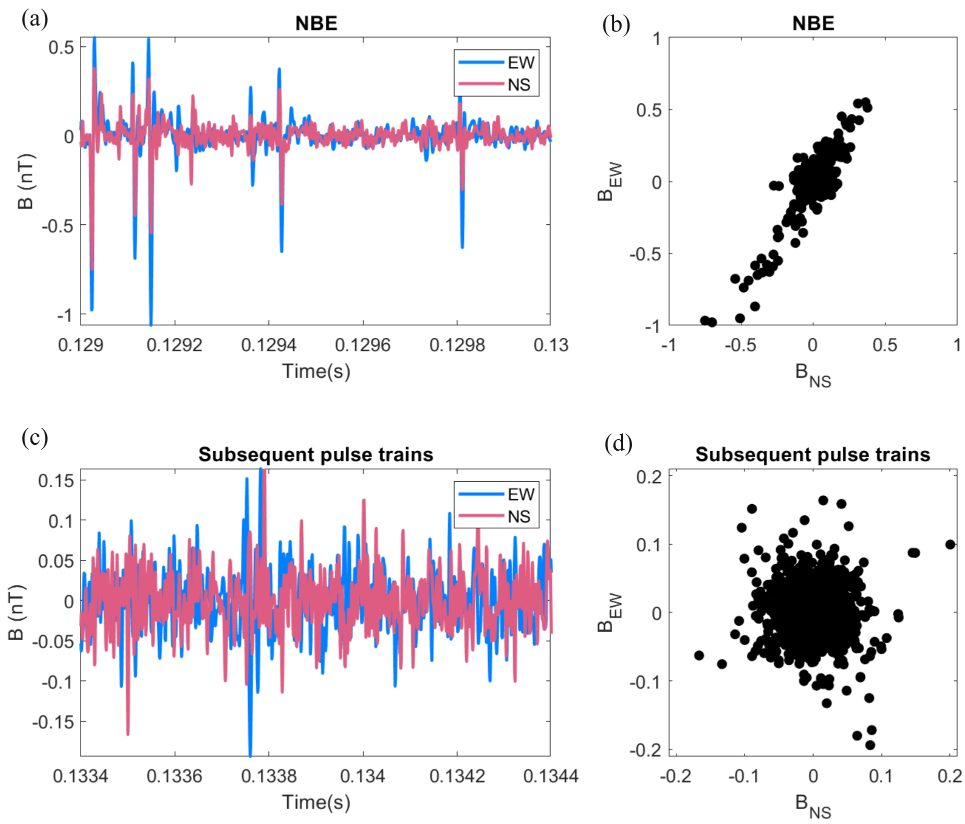

Figure S19. Similar to Figure S11, but for both NBE and its second subsequent pulse for event 8.

References

Alken, P., Thébault, E., Beggan, C. D., Amit, H., Aubert, J., Baerenzung, J., ... others (2021). International geomagnetic reference field: the thirteenth generation. *Earth, Planets and Space*, *73*(1), 1–25. doi: 10.1186/s40623-020-01288-x

Bilitza, D., Altadill, D., Zhang, Y., Mertens, C., Truhlik, V., Richards, P., ... Reinisch, B. (2014). The international reference ionosphere 2012–a model of international collaboration. *Journal of Space Weather and Space Climate*, *4*, A07. doi: 10.1051/swsc/2014004

Cummer, S. A. (2003). Current moment in sprite-producing lightning. *Journal of Atmospheric and Solar-Terrestrial Physics*, *65*(5), 499-508. (Sprites, Elves and their Global Activities) doi: https://doi.org/10.1016/S1364-6826(02)00318-8

Cummer, S. A., & Inan, U. S. (2000). Modeling elf radio atmospheric propagation and extracting lightning currents from elf observations. *Radio Science*, *35*(2), 385-394. doi: https://doi.org/10.1029/1999RS002184

Koshak, W. J., Solakiewicz, R. J., Phanord, D. D., & Blakeslee, R. J. (1994). Diffusion model for lightning radiative transfer. *Journal of Geophysical Research: Atmospheres*, *99*(D7), 14361-14371. doi: https://doi.org/10.1029/94JD00022

Lehtinen, N. G., & Inan, U. S. (2008). Radiation of elf/vlf waves by harmonically varying currents into a stratified ionosphere with application to radiation by a modulated electrojet. *Journal of Geophysical Research: Space Physics*, *113*(A6), A06301. doi: https://doi.org/10.1029/2007JA012911

Lehtinen, N. G., & Inan, U. S. (2009). Full-wave modeling of transionospheric propagation of vlf waves. *Geophysical Research Letters*, *36*(3), L03104. doi: https://doi.org/10.1029/2008GL036535

Li, D., Liu, F., Pérez-Invernón, F. J., Lu, G., Qin, Z., Zhu, B., & Luque, A. (2020). On the accuracy of ray-theory methods to determine the altitudes of intracloud electric discharges and ionospheric reflections: Application to narrow bipolar events. *Journal of Geophysical Research: Atmospheres*, *125*(9), e2019JD032099. doi: https://doi.org/10.1029/2019JD032099

Luque, A., Gordillo-Vázquez, F. J., Li, D., Malagón-Romero, A., Pérez-Invernón, F. J., Schmalzried, A., … Østgaard, N. (2020). Modeling lightning observations from space-based platforms (Cloudscat.jl 1.0). *Geoscientific Model Development*, *13*(11), 5549–5566. doi: https://doi.org/10.5194/gmd-13-5549-2020

Soler, S., Pérez-Invernón, F. J., Gordillo-Vázquez, F. J., Luque, A., Li, D., Malagón-Romero, A., … Østgaard, N. (2020). Blue optical observations of narrow bipolar events by ASIM suggest corona streamer activity in thunderstorms. *Journal of Geophysical Research: Atmospheres*, *125*(16), e2020JD032708. doi: 10.1029/2020JD032708

Uman, M. A., McLain, D. K., & Krider, E. P. (1975). The electromagnetic radiation from a finite antenna. *American Journal of Physics*, *43*(1), 33-38. doi: 10.1119/1.10027

Wilkman, O. (2013). *MieScatter,*. `https://github.com/dronir/MieScatter.jl`. ([Online; accessed 15 Jun 2020])